Contrib. Astron. Obs. Skalnaté Pleso **54/1**, 20 – 35, (2024)
https://doi.org/10.31577/caosp.2024.54.1.20

Negative and positive superhumps of V503 Cyg as seen in TESS data. I. Seasons 2019 and 2021

E. Pavlenko[1], **N. Pit**[1] **and T. Kato**[2]

[1] *Crimean astrophysical observatory of RAS, Crimea (E-mail: eppavlenko@gmail.com)*

[2] *Department of Astronomy, Kyoto University, Kyoto 606-8502, Japan*

Received: October 6, 2023; Accepted: December 7, 2023

Abstract. We report the TESS observations of the SU UMa-type dwarf nova V503 Cyg in 2019 and 2021 during a superoutburst, normal outbursts and quiescence. We identified stage A of the growing superhumps and stage B in positive superhump evolution. We found that the stage A lasted $\sim$ 0.8 d; during stage B a mean period of 0.081367(93) d decreased with the derivative $P_{dot}/P = -4.8*10^{-5}$. We estimated the mass ratio $q = 0.195$ using a fractional period excess for stage B. The quiescent state was represented by a strong signal at negative superhumps and a weak one at the orbital period. We detected a gradual increase of the 0.076-d period of negative superhumps in quiescence preceding normal outbursts in 2019 and 2021, and an abrupt decrease of the period during normal outbursts. This means that the radius of the accretion disk increases sharply during the outburst and gradually decreases towards the onset of the next outburst. Such behavior is consistent with the thermal-tidal instability model.

We found that the light curve folded on the orbital period shows a profile that changes from double-peak to single-peak, respectively, in the tilted and non-tilted state of the accretion disk. We speculate that this difference may be caused by a state of the accretion disk: in the tilted disk state, one spot is the hot spot on the edge of the disk, while another one may be a spot caused by the matter hitting the inner disk. During the non-tilted disk state, there is one spot on its edge.

Key words: accretion, accretion disks – cataclysmic variables – stars: dwarf novae – stars: individual: V503 Cyg

1. Introduction

SU UMa type dwarf novae are a subtype of cataclysmic variables with orbital periods ranging from $\sim$ 76 minutes to 3 hours and a mass ratio of $\leq$ 0.25 (Warner, 1995; Whitehurst, 1988; Lubow, 1991). They exhibit two types of outbursts: "normal" outbursts, lasting 2-3 days, caused by the thermal instability of the accretion disk and "superoutbursts", lasting 10-20 days, caused by the thermal-tidal instability model (Osaki, 1989, 1996). Normal outbursts are more frequent events and are localized between superoutbursts. The disk matter accretes (but

not completely) onto the white dwarf during each normal outburst (for general information on cataclysmic variables and dwarf novae, see e.g. Warner (1995)), thus, by the beginning of the next outburst, the radius of the disk R_d is larger than at the beginning of the previous one, and eventually it reaches a 3:1 resonant radius $R_d < 0.47$a, where a is the binary separation at which a tidal instability is triggered and a superoutburst occurs. The disk begins to precess in the orbital plane (prograde apsidal precession). As a result of precession, so-called positive superhumps (the wave-like changes in brightness with varying amplitudes, up to several tenths of a magnitude) appear, the period P_{sh} of which is several percents larger than the orbital one. This period is related to the orbital period P_{orb} and the precession period P_{prec} by the relation

$$1/P_{prec} = 1/P_{orb} - 1/P_{sh}. \quad (1)$$

Period of positive superhumps systematically varies: it is constant and biggest during the superhumps growing (stage A), variable during the next stage B and shorter, stable at a late stage C (Kato et al., 2009).

Another type of accretion disk precession is the retrograde nodal precession, probably caused by an accretion disk tilted to the orbital plane (Montgomery & Martin, 2010; Wood et al., 2011). This precession results in negative superhumps with a period slightly shorter than the orbital one. While positive superhumps are an attribute of cataclysmic variables with a mass ratio ≤ 0.3, the negative superhumps can appear in systems with any mass ratio (Montgomery, 2010). However, there are far fewer known cataclysmic variables with negative superhumps than with positive ones.

V503 Cyg is an active dwarf nova of the SU UMa type (Harvey et al., 1995). Its orbital period obtained from both radial vilocity (Harvey et al., 1995) and photometry (Pavlenko et al., 2012) is 0.07776 d, the interval between superoutbursts (supercycle) is 89 d. The interval between adjacent normal outbursts (cycle) varied from 7 to 30 d on a scale of ~ 20 years. Negative superhumps with a period of 0.076 d were found by Harvey et al. (1995) and Szkody et al. (1989) in epoch of infrequent outbursts. Later a disappearance of negative superhumps was recorded by Pavlenko et al. (2012) along with a decrease in the normal cycle to 8-9 d. Yet in 2002 Kato et al. (2002) noticed a decrease in the normal cycle of V503 Cyg. This was an observational confirmation of the idea of Osaki & Kato (2013b) about the appearance/disappearance of negative superhumps with the lengthening/reduction of the normal cycle. Information about V503 Cyg state (with or without a disk tilt) and periodic processes for different years is presented in Table 1.

2. Observations

Observations of the V503 Cyg were carried out by the NASA Transiting Exoplanet Survey Satellite (TESS) during two seasons at 2-min cadence. The first

Table 1. V503 state and types of periodicity

Binary state	Cycle	Period	Reference
With disk tilt		Negative superhumps 0.0760 d	Szkody et al. (1989)
With disk tilt	30 d	Negative superhumps 0.075694 d	Harvey et al. (1995)
		Positive superhumps 0.081041 d	-"-
		Orbital 0.077708 d	-"-
Without disk tilt	7-9 d		Kato et al. (2002)
Without disk tilt	8-9 d	Orbital 0.077760 d	Pavlenko et al. (2012)
Without disk tilt		Orbital 0.0777591 d	Kato et al. (2014)
Without disk tilt		Positive superhumps 0.081446 d	-"-

season took place in 2019 between JD 2458683 and 2458737. The second season occured in 2021 between JD 2459420 and 2459446. The TESS band-pass is wide $\sim 600 - 1,000$ nm, see Ricker et al. (2015) for a description of TESS.

3. Results

3.1. V503 Cyg long-term light curves

The long-term light curve of V503 Cyg is presented in Fig. 1. It includes the

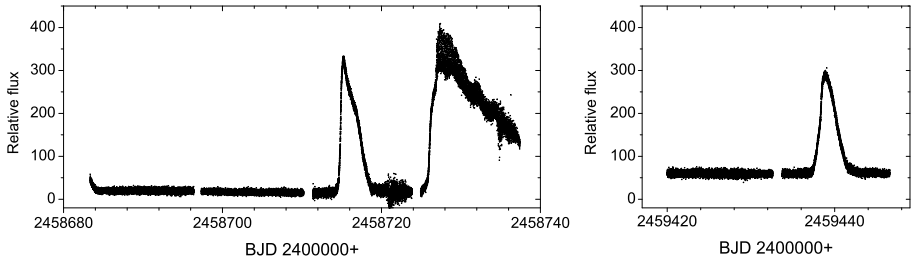

Figure 1. The overall light curve in 2019 (left) and 2021 (right). Data are expressed in relative flux.

superoutburst, a normal outburst, a quiescent state around and in between in 2019, a normal outburst and quiescent state around it in 2021. The total duration of both normal outbursts was about four days, but their profiles were different. The 2019 outburst has a sharper increase in brightness compared to decrease, so it is an "outside-in" type outburst, and the 2021 outburst is

rather an "inside-out" type one (Smak (1984)). According to the AAVSO data, a slight excess of brightness at the beginning of TESS 2019 set of observations corresponds to the end of the normal outburst. So one can conclude that the time between two normal outbursts (a normal cycle) was about 34 days which is comparable to the 30-day normal cycle recorded by Harvey et al. (1995) in the era of negative superhumps in the 1994 quiescence.

3.2. Periodicity in outbursts and quiescence

During all states of the V503 Cyg activity a short-term periodicity around 1.8 – 2 hours has been observed. Some examples of the light curves in the quiescence, the normal outburst and the superoutburst are shown in Fig. 2.

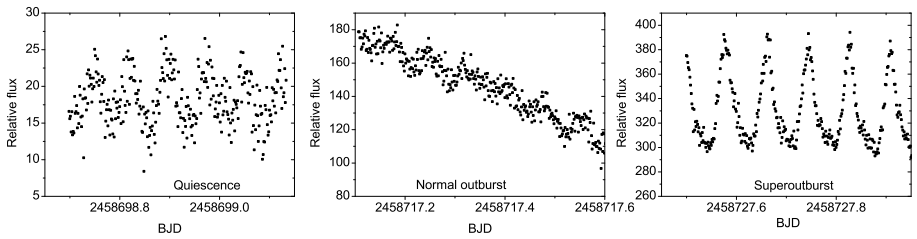

Figure 2. Examples of the light curves during the quiescence, the normal outburst and the superoutburst. Data are expressed in the relative flux.

As expected, the brightness changes in the quiescent state occurred with a different period than in the superoutburst. This is illustrated in Fig. 3, where there are the periodograms computed by the Stellingwerf method implemented in the ISDA package by Pel't (1980) for the quiescent state that preceded the 2019 normal outburst and for the 2019 superoutburst. It can be seen from the periodograms that an average period of brightness variations during the superoutburst was 0.081367(93) days, while in the quiescence it was 0.076063(12) days. These values are close to the periods of positive and negative superhumps, respectively, registered earlier (see Table 1). Broad peaks indicate that both periods have undergone changes over time. The continuity of observations provided by TESS made it possible to determine the frequencies of brightness changes in rather narrow time ranges; in this case, the duration of each range was 0.8 d, which ensured the accuracy of determining the period in the 4th decimal place. The result is presented in Fig. 4. The graphs show that the periods of both types of superhumps do change with time, but the nature of these changes is different. Let us consider the changes in positive and negative superhumps in more detail.

3.2.1. Evolution of positive superhumps and mass ratio

To identify the stages of the positive superhumps evolution for the 2019 superoutburst, we have determined the moments of maximum brightness of positive superhumps *MaxBJD* and calculated the values of O-C using the ephemeris

$$MaxBJD = 2458726.51 + 0.08145 * E. \quad (2)$$

Fig. 5 shows the O-C values along with superhump amplitudes and the superoutburst light curve. The superoutburst started with a precursor in a form of a

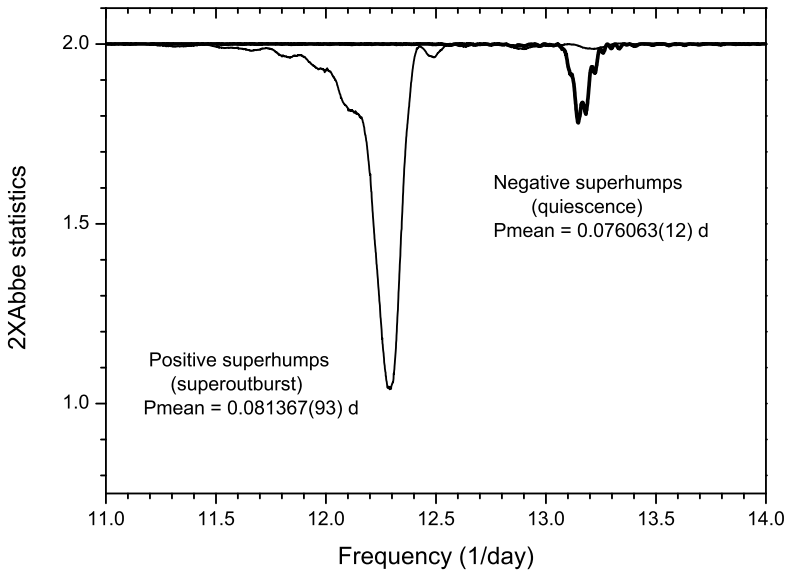

Figure 3. The periodograms for the superoutburst (thin line) and the 2019 quiescence (bold line). The peaks point to the mean period of positive superhumps in the superoutburst and negative superhumps in the quiescence that is limited by the normal outburst.

sharp brightness increase lasting a third of a day, followed by a slower brightening that lasted about 0.7 day and a sloping plateau with duration of at least 10 days (see Fig. 6). The precursor is thought as a normal outburst launching a superoutburst. As it can be seen in the bottom panel of Fig. 6, superhumps appeared already at the precursor stage. The fact that the superhumps appeared not at the main superoutburst, but at the precursor stage confirms the validity of a thermal-tidal instability theory (Osaki, 1996). From the beginning of the appearance of superhumps until they reached their maximum amplitude, only 10 cycles passed. We identified this interval as stage "A" (Kato et al.,

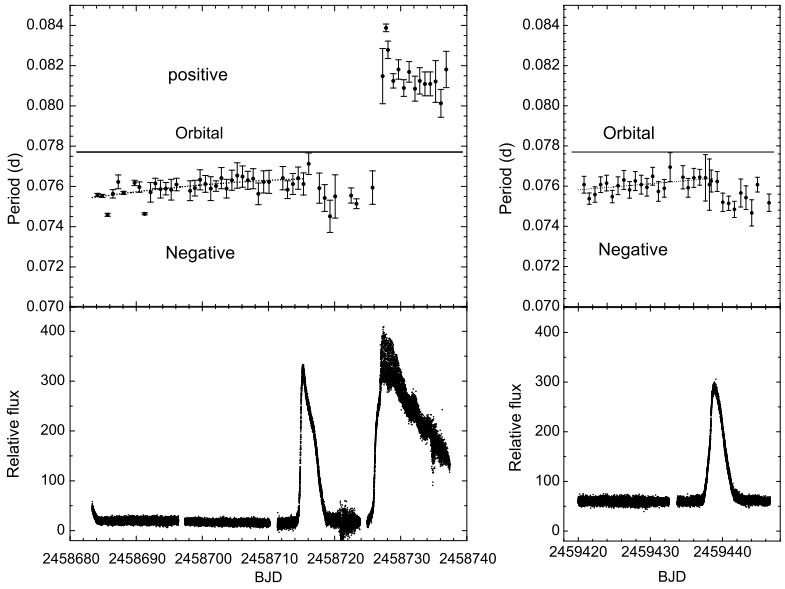

Figure 4. Upper panel: the period of negative superhumps in the quiescence and positive superhumps in the superoutburst. Lower panel: 2019 and 2021 light curves.

2009) of the positive superhumps growing and, approximating this O-C segment with a straight line, determined the period of superhumps to be equal to $P_A = 0.08247(51)$ d. For this period, we found a fractional period excess $\epsilon^* = 0.057$ (~ 0.8 d) using the relation proposed by Kato & Osaki (2013),

$$\epsilon^* = 1 - P_{orb}/P_A. \tag{3}$$

Having reached the maximum amplitude, the superhumps entered stage "B". During this stage, the amplitude of superhumps decreased, the period also decreased with a derivative of $P_{dot}/P = -4.8 * 10^{-5}$.

Note that the period at extremely short stage A may be distorted due to the influence of previous negative superhumps and the subsequent influence of positive superhumps at stage B. A situation, when for some reason the period at stage A is not correctly determined, was considered by Kato (2022). He proposed to use the empirical relation between the mass ratio at the resonant radius of 3:1 and ϵ at stage B:

$$\epsilon = (P_{sh} - P_{orb})/P_{orb}, \tag{4}$$

where P_{sh} is the mean period of positive superhumps at the stage B. In our case, the average period at the plateau stage (stage B) is 0.08137 d and the orbital period 0.0777591 d give $\epsilon = 0.046$ and q = 0.195 (from Table 4 in Kato (2022)).

Fig. 7 illustrates in detail how the positive superhumps evolved during the stage "B" for each interval of the inclined superoutburst plateau when

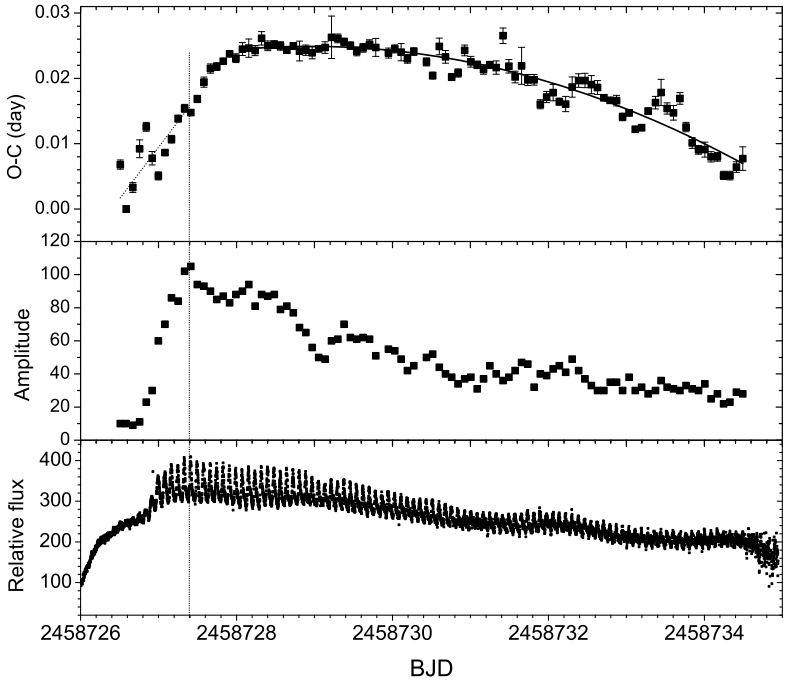

Figure 5. O-C of positive superhumps maxima (upper panel), their amplitudes (middle panel) and the superoutburst light curve shown in the top, middle and bottom panel respectively. The vertical line separates the stages "A" and "B" of the positive superhumps development.

it is divided into four intervals: BJD=2458727.08-2458728.95 (a), 2458729.27-2458730.73 (b), 2458731.33-2458732.93 (c) and 2458733.33-2558734 (d). Periodograms show the decrease of periods: the average values of the period are $P_a = 0.08211(18)$; $P_b = 0.08110(23)$; $P_c = 0.08126(21)$; $P_d = 0.08087(26)$ in these intervals. The corresponding phase curves show decrease of the amplitude and profile changes along the superoutburst plateau. As in earlier observations (Kato et al., 2014), the profile was a single peak at the beginning of the superoutburst and became a double peak one at the end of the superoutburst.

Next, we carried out the prewhitening procedure by subtracting the light variations corresponding to each interval with a period of positive superhumps. The periodograms constructed for the data residuals are shown in Fig. 8. The residual light variations in the first interval (a) are close to the orbital frequency F_{orb} and the beat period $2F^+ - F_{orb}$, where F^+ is the average frequency of positive superhumps in this interval. The second interval (c) does not contain any significant frequencies and the corresponding periodogram is not shown

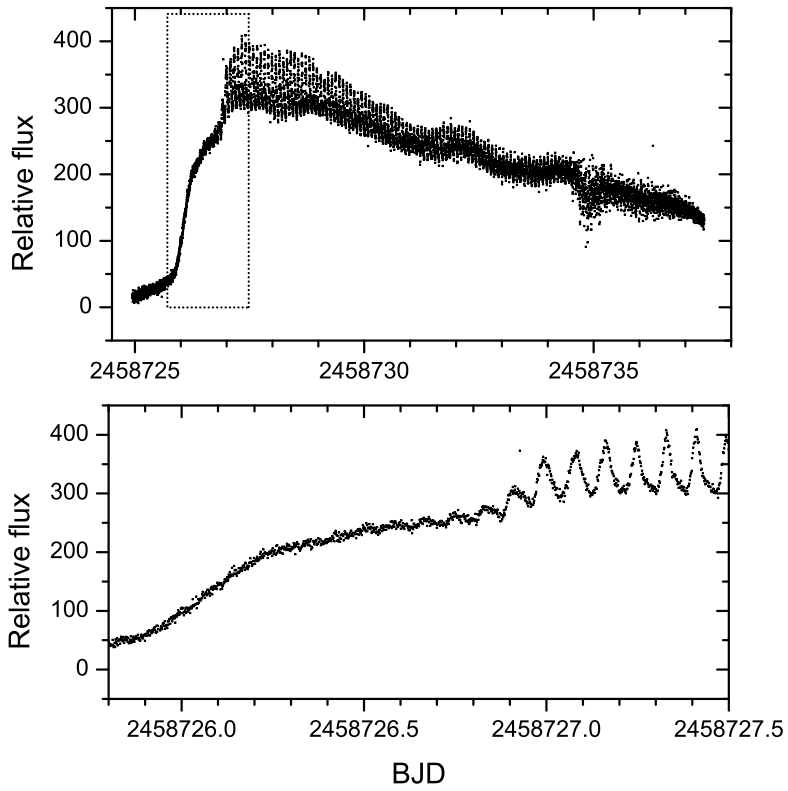

Figure 6. The superoutburst (upper panel). Its fragment, demonstrating the appearance and development of positive superhumps, is marked with a rectangle and shown in more detail in the bottom panel.

in the figure. Periodograms for the third (c) and fourth intervals (d) have a slight excess of the signal in the vicinity of the average frequency of negative superhumps. This may indicate that negative superhumps also exist during a supeoutburst, but they are hardly distinguishable against the background of the overwhelming power of positive superhumps.

3.2.2. Evolution of negative superhumps

As it was seen in Fig 4, negative superhumps between neighboring normal outbursts in 2019 (JD ∼2458684 – ∼2458711) show a gradual increase in the period (decrease in frequency). During the outburst, which began on JD 2458711, there is a sharp increase in frequency, which slowly decreases after the end of the outburst. The same behavior is observed for the 2021 outburst. The pattern of a

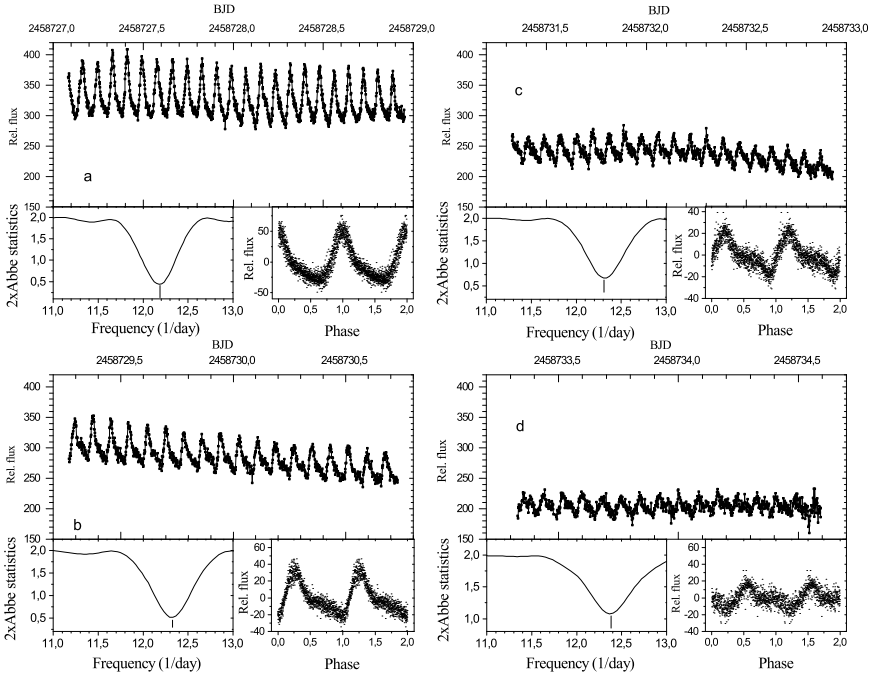

Figure 7. Original light curves, corresponding periodograms and phase light curves for different parts "a", "b", c" and "d" (see the explanations in the text) of the superoutburst plateau. The time of the first measurement in each interval was taken as the initial epoch, i.e. BJD 2458727.08448 for interval a, 2458729.27059 for b, 2458731.32892 for c and 2458733.33031 for d.

frequency change is similar to what Osaki and Kato found in the Kepler dwarf nova V1504 Cyg (Osaki & Kato, 2013b).

We also analyzed the period variation in both normal outbursts and their vicinity in more detail using the O-C method. In this case, for the brightness maxima of the negative superhumps for the first normal outburst, we used the ephemeris

$$MaxHJD = 2458711.398 + 0.07616 * E \tag{5}$$

and for the second - ephemeris

$$MaxHJD = 2459433.778 + 0.07616 * E. \tag{6}$$

The O-C course for both normal outbursts is shown in Fig.9. In both cases, at the maximum of each normal outburst, there was an abrupt decrease in the period (increase in frequency) of negative superhumps. After the end of each outburst, the period gradually increased during a normal cycle (see Fig. 4). A

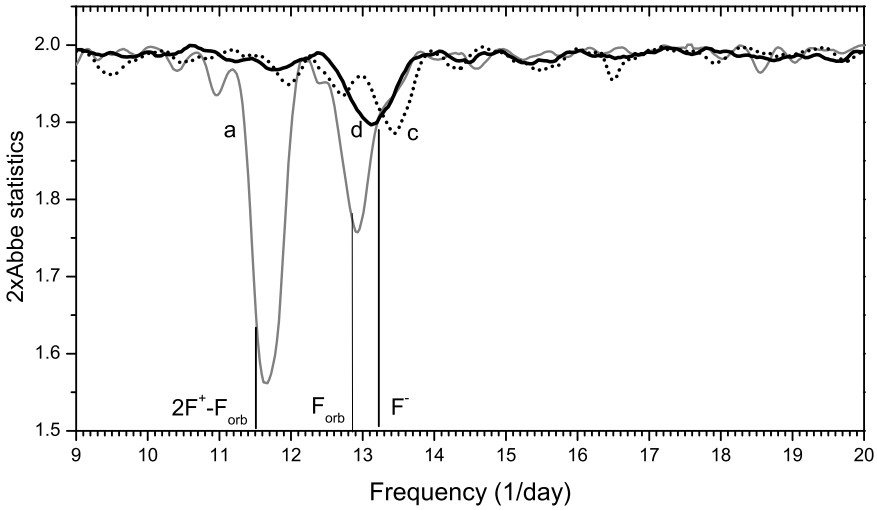

Figure 8. Periodograms for the prewhitened data at different parts "a", "c" and "d" of the superoutburst plateau. The position of the orbital frequency and combination of positive superhumps and orbital variations frequencies is marked by lines. The region of negative superhumps is shown by the grey streap.

similar behavior was first observed in the Kepler V1504 Cyg by Osaki & Kato (2013b).

3.2.3. Orbital modulation

Although there is no prominent evidence of the orbital period in the periodogram presented in Fig. 3, we decided to check this more carefully: to remove the mean negative superhump period from the all the quiescent TESS data and to analyse residuals. The resulting periodogram does contain a weak signal at the orbital period (Fig.11, left) that is hidden in the periodogram of Fig. 3. Note that this mean light curve profile ("orbital light curve") is a two-humped one, with humps separated by half a period. The amplitude of a larger hump is about $0^m.06$. However, the orbital profile in the epoch of the orbital period dominance and the absence of negative superhumps in the 2010 (Pavlenko et al., 2012) and 2011-2012 quiescence states without a disk tilt (Kato et al., 2013) (see Fig.11, right) is one-humped with an amplitude of $\sim 0^m.2$.

To see a potential change of the waveform of orbital variation during the quiescence, we calculated periodograms for several selected intervals of the 2019 and 2021 quiescence (see Fig. 12). One could see that while the larger hump is stable at all intervals, the smaller hump displays a slightly variable amplitude.

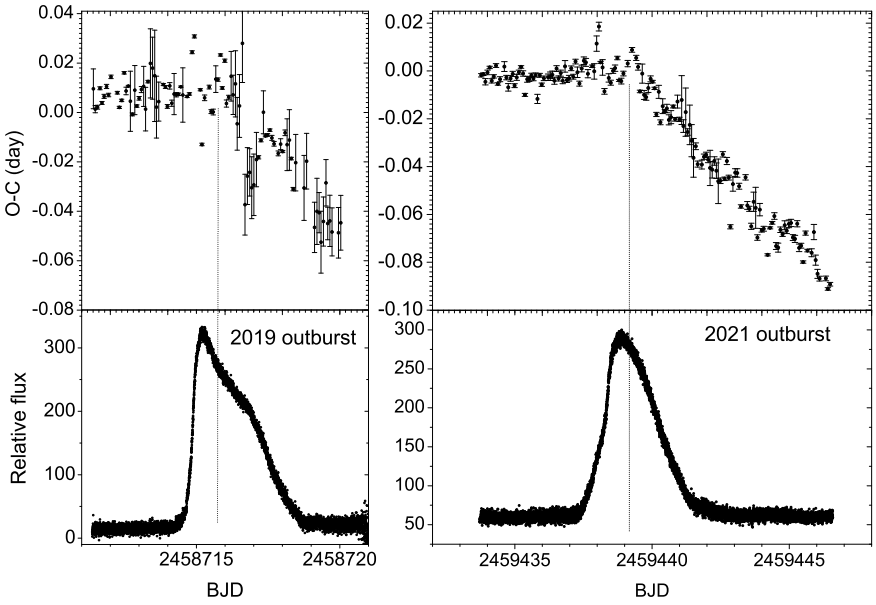

Figure 9. O-C of the negative superhumps maxima (top) and the corresponding light curves. The line is drawn through a sharp change in the O-C behavior.

4. Discussion

4.1. Accretion disk radius

According to Larwood (1998), the frequency of negative superhumps is related to the radius of the accretion disk by a simplified relation

$$\nu_{neg}/\nu_{orb} = 1 + \eta * 3/7(q/(1+q)^{1/2}) * (R_d/a)^{3/2} * cos\theta, \quad (7)$$

where ν_{neg} is the frequency of negative superhumps; ν_{orb} is the orbital frequency, q is the mass ratio, $cos\theta$ ~1 for a small disk inclination angle, a is the binary separation, and η is a correction factor depending on the distribution of matter density in the disk. Reconciliation of this formula to the evolution of negative superhumps found by us shows that the radius of the accretion disk abruptly increases during the normal outburst and gradually decreases towards the onset of a next outburst. Similar phenomena were obtained for the Kepler V1504 Cyg (Osaki and Kato) and for the ground-based observations of MN Dra (Sklyanov et al., 2020), and NY Her (Pavlenko et al., 2021). Such behavior of the accretion disk is in accordance with the prediction of the thermal-tidal instability model.

As for the estimation of the disk radius, we have to know the correction factor η, which is unknown for the V503 Cyg in quiescence. Using equation (7) for q=0.195, ν_{orb} = 12.86, the mean frequencies of negative superhumps ν_{neg}

= 13.20(4) and 13.09(5); ν_{neg} = 13.20(4) and 13.09(4) at the start and the end of the 2019 and 2021 quiescence, we calculated the dependence of the disk radius on η (see Fig. 10). The range of probable disk radius values is limited by the possible η=1.94-2.12 (Osaki & Kato, 2013a) and the 3:1 resonant radius unattainable in a normal outburst. One could see that a larger η corresponds to smaller radii. Despite of an unknown density distribution of matter in the V503 Cyg disk, we can take η = 1.22 that Osaki & Kato (2013a) assumed for the quiescent disk of the Kepler V1504 Cyg. In this case we obtain in average a decrease of the disk radius from 0.43(3)a to 0.33(4)a during the quiescent state between two normal outbursts (Fig. 10). Although these values may look close to reality (see, for example, a discussion in Hellier (2001), we still cannot assert their truth due to the unknown real density distribution of matter in the disk.

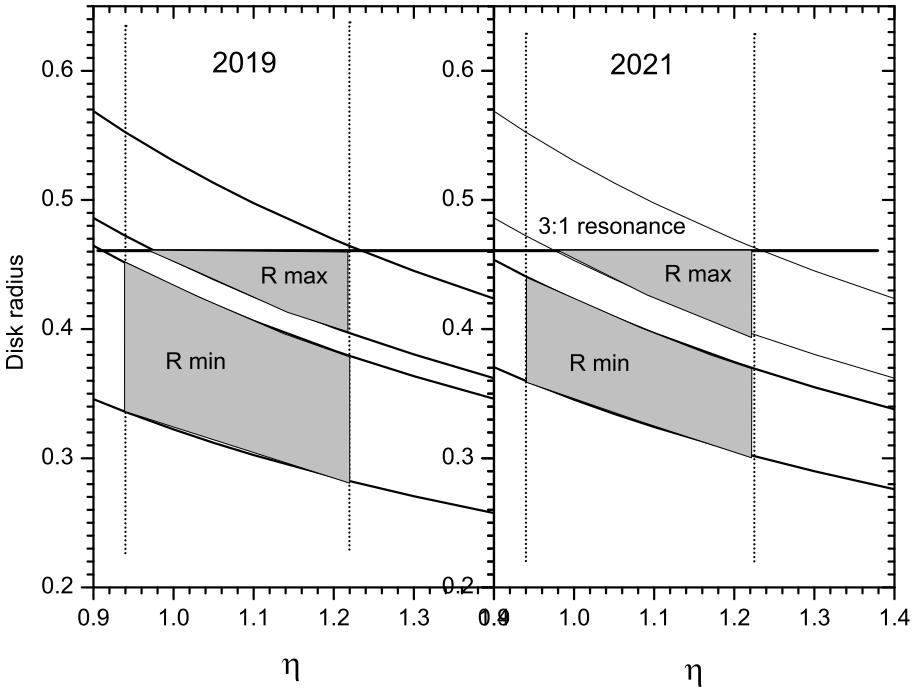

Figure 10. Dependence of the disk radius on a correction factor η for 2019 and 2021 years. The disk radius is expressed in the binary separation "a". The range of possible radius values is shown in gray. The horizontal line corresponds to the 3:1 resonant radius.

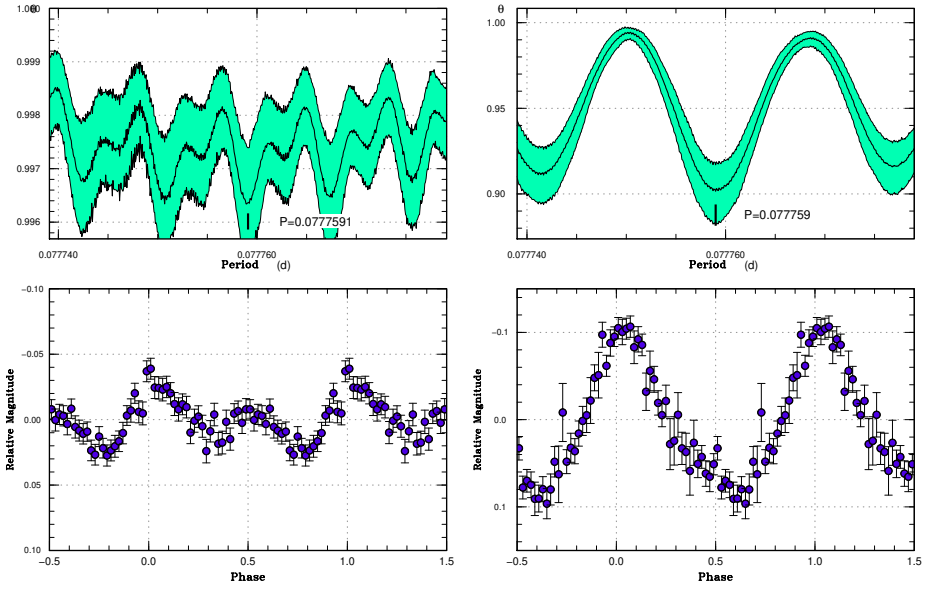

Figure 11. Orbital period. Periodograms and data folded on the orbital period for all the quiescent TESS data (left) and those for the 2011-2012 quiescence (right).

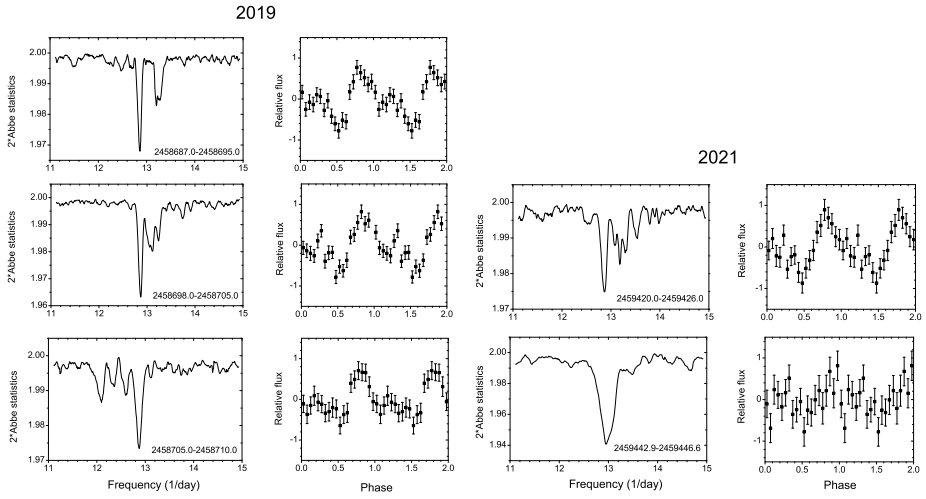

Figure 12. Orbital period. Periodograms and data folded on the orbital period for the selected quiescent TESS data in 2019 (left) and 2021 quiescence (right). The zero-epoch is 2458687.00118 and $Porb = 0.0777591$ d.

4.2. Difference of orbital light curve profile in tilted and non-tilted disk state

A potential contribution of various sources of radiation in CVs to the total radiation of the system may differ in different CVs, and this determines the waveform of orbital modulation. A "typical" profile of the light curve folded on the orbital period is one-humped due to a hot spot on the rim of the accretion disk. However, there are some exceptions. A one-humped light curve may be caused also by a reflection effect of the secondary component. Among cataclysmic variables there are cases of double-humped light curves with different interpretation. They may imply the contribution of ellipsoidality of a secondary, or a spiral structure of the accretion disk in the dwarf novae with a low mass ratio, predicted by Lin & Papaloizou (1979). Dai et al. (2018) suggested that double-humped orbital modulation in the systems with low inclination may be caused by two spots – one on the edge of disk, the other on its surface.

We believe that the change in the V503 Cyg orbital light curve profile is due to a change in the state of the accretion disk. As Kimura et al. (2020) noted, that contrary to the typical case of a non-tilted disk, in binaries with a tilted disk, the accretion stream not only hits the outer rim of the disk, but also reaches the inner part of the disk. The two-humped orbital profile of the TESS data may be due to the fact that in the state with a disk tilt, one spot appears to be the hot spot on the edge of disk, while another may be from a spot caused by the matter hitting an inner disk. During the state without a disk tilt, there is one spot on the edge of disk.

5. Conclusion

We analysed the photometric data of the SU UMa-type dwarf nova V503 Cyg obtained in 2019 and 2021 with the Transiting Exoplanet Survey Satellite (TESS). The main results are summarized as follows:

- The A and B stages in the positive superhumps evolution during the 2019 superoutburst were identified and the mass ratio was estimated.

- In 2019 and 2021 the strong negative superhumps dominanted during the quiescence and normal outbursts, so the binary state of V503 Cyg was with an accretion disk tilt. The period of negative superhumps showed cyclical changes: it increased slowly between normal outbursts and decreased sharply during the outburst. This reflects cyclic changes in the radius of the disk, consistent with the thermal-tidal instability model.

- It was found that in the 2019 quiet state a weak signal was detected at the orbital period. Its profile was double-humped, as opposed to the single-humped one observed in the era when the orbital signal was dominant. We hypothesized that the difference in profiles could be due to the different state of the binary system. The one-humped profile is caused by a hot spot on the edge of the non-

titled disk, and the two-humped one is associated with one spot on the edge of a tilted disk, and the second spot - in its inner part.

Acknowledgements. The authors are grateful to the reviewer Sergey Shugarov for a careful reading of the manuscript, comments, and a discussion.

References

Dai, Z., Szkody, P., Kennedy, M., et al., A Phenomenological Model for the Light Curve of Three Quiescent Low-inclination Dwarf Novae and One Pre-cataclysmic Variable. 2018, *Astronomical Journal*, **156**, 153, DOI: 10.3847/1538-3881/aadb99

Harvey, D., Skillman, D. R., Patterson, J., & Ringwald, F. A., Superhumps in Cataclysmic Binaries. V. V503 Cygni. 1995, *Publications of the ASP*, **107**, 551, DOI: 10.1086/133591

Hellier, C. 2001, *Cataclysmic Variable Stars*

Kato, T., Evolution of short-period cataclysmic variables: implications from eclipse modeling and stage A superhump method (with New Year's gift). 2022, *arXiv e-prints*, arXiv:2201.02945, DOI: 10.48550/arXiv.2201.02945

Kato, T., Hambsch, F.-J., Maehara, H., et al., Survey of Period Variations of Superhumps in SU UMa-Type Dwarf Novae. IV. The Fourth Year (2011-2012). 2013, *Publications of the ASJ*, **65**, 23, DOI: 10.1093/pasj/65.1.23

Kato, T., Hambsch, F.-J., Maehara, H., et al., Survey of period variations of superhumps in SU UMa-type dwarf novae. V. The fifth year (2012-2013). 2014, *Publications of the ASJ*, **66**, 30, DOI: 10.1093/pasj/psu014

Kato, T., Imada, A., Uemura, M., et al., Survey of Period Variations of Superhumps in SU UMa-Type Dwarf Novae. 2009, *Publications of the ASJ*, **61**, S395, DOI: 10.1093/pasj/61.sp2.S395

Kato, T., Ishioka, R., & Uemura, M., Dramatic Changes in the Outburst Properties in V503 Cygni. 2002, *Publications of the ASJ*, **54**, 1029, DOI: 10.1093/pasj/54.6.1029

Kato, T. & Osaki, Y., New Method of Estimating Binary's Mass Ratios by Using Superhumps. 2013, *Publications of the ASJ*, **65**, 115, DOI: 10.1093/pasj/65.6.115

Kimura, M., Osaki, Y., Kato, T., & Mineshige, S., Thermal-viscous instability in tilted accretion disks: A possible application to IW Andromeda-type dwarf novae. 2020, *Publications of the ASJ*, **72**, 22, DOI: 10.1093/pasj/psz144

Larwood, J., On the precession of accretion discs in X-ray binaries. 1998, *Monthly Notices of the RAS*, **299**, L32, DOI: 10.1046/j.1365-8711.1998.01978.x

Lin, D. N. C. & Papaloizou, J., Tidal torques on accretion discs in binary systems with extreme mass ratios. 1979, *Monthly Notices of the RAS*, **186**, 799, DOI: 10.1093/mnras/186.4.799

Lubow, S. H., A Model for Tidally Driven Eccentric Instabilities in Fluid Disks. 1991, *Astrophysical Journal*, **381**, 259, DOI: 10.1086/170647

Montgomery, M., Earth, Moon, Sun, Accretion Disks, And Retrograde Precession. 2010, in American Astronomical Society Meeting Abstracts, Vol. **215**, *American Astronomical Society Meeting Abstracts #215*, 301.07

Montgomery, M. M. & Martin, E. L., A Common Source of Accretion Disk Tilt. 2010, *Astrophysical Journal*, **722**, 989, DOI: 10.1088/0004-637X/722/2/989

Osaki, Y., A model for the superoutburst phenomenon of SU Ursae MAjoris stars. 1989, *Publications of the ASJ*, **41**, 1005

Osaki, Y., Dwarf-Nova Outbursts. 1996, *Publications of the ASP*, **108**, 39, DOI: 10.1086/133689

Osaki, Y. & Kato, T., Study of Superoutbursts and Superhumps in SU UMa Stars by the Kepler Light Curves of V344 Lyrae and V1504 Cygni. 2013a, *Publications of the ASJ*, **65**, 95, DOI: 10.1093/pasj/65.5.95

Osaki, Y. & Kato, T., The Cause of the Superoutburst in SU UMa Stars is Finally Revealed by Kepler Light Curve of V1504 Cygni. 2013b, *Publications of the ASJ*, **65**, 50, DOI: 10.1093/pasj/65.3.50

Pavlenko, E. P., Samsonov, D. A., Antonyuk, O. I., et al., Photometry of the dwarf nova V503 Cyg in 2010. Orbital and other periods. 2012, *Astrophysics*, **55**, 494, DOI: 10.1007/s10511-012-9255-4

Pavlenko, E. P., Sosnovskii, A. A., Antonyuk, K. A., et al., Changes in the Period of Negative Superhumps of Type SU UMa Dwarf Novae. II. NY Her (2017 and 2020). 2021, *Astrophysics*, **64**, 293, DOI: 10.1007/s10511-021-09690-3

Pel't, Y. 1980, *Frequency analysis of astronomical time series.*

Ricker, G. R., Winn, J. N., Vanderspek, R., et al., Transiting Exoplanet Survey Satellite (TESS). 2015, *Journal of Astronomical Telescopes, Instruments, and Systems*, **1**, 014003, DOI: 10.1117/1.JATIS.1.1.014003

Sklyanov, A. S., Pavlenko, E. P., Antonyuk, K. A., et al., Variations in the Period of Negative Superhumps in SU UMa-Type Dwarf Novae. I. Mn Dra (2012-2017). 2020, *Astrophysics*, **63**, 200, DOI: 10.1007/s10511-020-09626-3

Smak, J., Accretion in cataclysmic binaries. IV. Accretion disks in dwarf novae. 1984, *Acta Astronomica*, **34**, 161

Szkody, P., Howell, S. B., Mateo, M., & Kreidl, T. J., CCD Time-Resolved Photometry of Faint Cataclysmic Variables. II. 1989, *Publications of the ASP*, **101**, 899, DOI: 10.1086/132550

Warner, B., Books-Received - Royal Observatory - Cape of Good Hope - 1820-1831 - the Founding of a Colonial Observatory. 1995, *Science*, **270**, 1859

Whitehurst, R., Numerical simulations of accretion discs - I. Superhumps : a tidal phenomenon of accretion discs. 1988, *Monthly Notices of the RAS*, **232**, 35, DOI: 10.1093/mnras/232.1.35

Wood, M. A., Still, M. D., Howell, S. B., Cannizzo, J. K., & Smale, A. P., V344 Lyrae: A Touchstone SU UMa Cataclysmic Variable in the Kepler Field. 2011, *Astrophysical Journal*, **741**, 105, DOI: 10.1088/0004-637X/741/2/105